Basic Science

JOURNAL OF CHILDREN'S ORTHOPAEDICS

Intraoperative 2D C-arm and 3D O-arm in children: a comparative phantom study

M. Prod'homme[1,2]
M. Sans-Merce[3,4]
N. Pitteloud[4,5]
J. Damet[4,6]
P. Lascombes[1,2]

Abstract

Purpose Exposure to ionizing radiation is a concern for children during intraoperative imaging. We aimed to assess the radiation exposure to the paediatric patient with 2D and 3D imaging.

Methods To evaluate the radiation exposure, patient absorbed doses to the organs were measured in an anthropomorphic phantom representing a five-year-old child, using thermoluminescent dosimeters. For comparative purposes, organ doses were measured using a C-arm for one minute of fluoroscopy and one acquisition with an O-arm. The cone-beam was centred on the pelvis. Direct and scattered irradiations were measured and compared (Student's *t*-test). Skin entrance dose rates were also evaluated.

Results All radiation doses were expressed in µGy. Direct radiation doses of pelvic organs were between 631.22 and 1691.87 for the O-arm and between 214.08 and 737.51 for the C-arm, and were not significant (p = 0.07). Close scattered radiation on abdominal organs were between 25.11 and 114.85 for the O-arm and between 8.03 and 55.34 for the C-arm, and were not significant (p = 0.07). Far scattered radiation doses on thorax, neck and head varied from 0.86 to 6.42 for the O-arm and from 0.04 to 3.08 for the C-arm, and were significant (p = 0.02). The dose rate at the skin entrance was 328.58 µGy.s^{-1} for the O-arm and 1.90 with the C-arm.

Conclusion During imaging of the pelvis, absorbed doses for a 3D O-arm acquisition were higher than with one minute fluoroscopy with the C-arm. Further clinical studies comparing effective doses are needed to assess ionizing risks of the intraoperative imaging systems in children.

Cite this article: Prod'homme M, Sans-Merce M, Pitteloud N, Damet J, Lascombes P. Intraoperative 2D C-arm and 3D O-arm in children: a comparative phantom study *J Child Orthop* 2018;12:550-557. DOI 10.1302/1863-2548.12.180016

Keywords: ionizing radiations; CBCT; O-arm; paediatric orthopaedics; patient exposure

[1]Medical University of Geneva, Geneva, Switzerland
[2]Paediatric Orthopaedic Division, Geneva University Hospital (HUG), Geneva, Switzerland
[3]Radiology Division, Geneva University Hospital (HUG), Geneva, Switzerland
[4]Institute of Radiation Physics, Lausanne University Hospital, Lausanne, Switzerland
[5]Physics Section, University of Geneva, Geneva, Switzerland
[6]Department of Radiology, University of Otago, Christchurch, New Zealand

Correspondence should be sent to M. Prod'homme, Paediatric Orthopaedic Division, Geneva University Hospital (HUG), Rue Willy-Donzé 6, CH-1211 Geneva, Switzerland.
E-mail: marcprod86@gmail.com

Introduction

Imaging is regularly needed in order to guide the surgeon during surgery in paediatric orthopaedics. The evolution of materials has led to safety improvements and effectiveness. However, radiation-induced injuries related to imaging devices remain a concern.[1] Numerous cohort studies about diagnostic and therapeutic irradiations[2] for benign diseases show a higher risk of thyroid,[3] breast,[4] brain[5] and skin[6] cancers, as well as leukemia.[7] Radiation exposure in children is especially concerning, as their higher sensitivity to radiation and longer life expectancy make them more likely to develop a radiation-induced cancer later in their lifetime.[2,8,9] Therefore, optimizing radiation exposure related to imaging devices is particularly important for the paediatric patient.

In the operating room, orthopaedic surgeons regularly use a fluoroscopic device, named the 'C-arm', which generates 2D images, useful to guide the intervention. A 3D image is advantageous for more precise and less invasive surgery.[10] The O-arm surgical imaging system (Medtronic, Fridley, Minnesota) is a 2D fluoroscopic and 3D volumetric imaging device utilized in the operating room.[11] After a 3D image scan is performed, the O-arm can be linked with a navigation system[12] in order to provide accurate guidance of surgical instruments in the operative field without additional irradiation. Several studies reported benefits of this technology, with increased surgical accuracy and higher patient safety.[13,14]

Nowadays, the doses generated by the C-arms and the O-arms are well-known, and several solutions exist regarding radiation dose reduction. For the operative

CT-scan, Su et al[15] published a study related to a low-dose protocol of imaging (80 kV, 80 mAs) named 'paediatric protocol', which permitted to divide by a factor of 10 the radiation doses, in comparison with a standard protocol.[15] Furthermore, Abul-Kasim et al[16] showed that the radiation doses of the O-arm could be reduced between five and 13 times without decreasing image quality within the framework of spine surgery. The work on polymethyl methacrylate (PMMA) phantoms from Petersen et al[17] found similar results.

To our knowledge, there are a few studies that quantify the irradiation level generated by the O-arm and by regular C-arm devices in children. Richerand et al[18] found a mean effective dose of 1.48 millisievert (mSv) with computerized navigation for pedicle screw placement *versus* 0.34 mSv with the use of the C-arm. One adult study has been recently published.[19] It is difficult to compare one O-arm acquisition and with the use of the C-arm. Su et al[20] mentioned the comparison of the paediatric low-dose O-arm with 85 seconds of C-arm fluoroscopy. A study on pedicle screw placement from Rampersaud et al[21] found the mean fluoroscopy time to be 9.3 seconds per screw. Furthermore, in the International Commission on Radiological Protection (ICRP) 117, the usual fluoroscopy time in common orthopaedic procedures such as intramedullary nailing of pertrochanteric fractures, open reduction and internal fixation of malleolar fractures, and intramedullary nailing of diaphyseal fractures of the femur ranges from 1.5 to 6.3 minutes.[22] Therefore, normalizing to one minute of fluoroscopy seems to be suitable for the comparison with one single acquisition of the O-arm.

Knowledge of doses received by organs during radiological interventions is important as different organs have different radio-sensitivities and susceptibilities to radiation-induced damages. Skin is particularly of concern, as it is the most severely affected during radiological examinations, with a threshold of burns and epilations of 2 Gy being the limit at which these effects begin to appear.[23]

The main goal of this study is to evaluate, via a child phantom, the organ dose of the direct and scattered irradiations that paediatric patients might potentially receive. A comparison between one minute of 2D C-arm and one 3D acquisition of the O-arm in a model of a pelvic irradiation was performed. The second goal of the study is the comparison of the skin dose rate between the classic 2D C-arm and the 2D produced with the O-arm.

Materials and methods

Materials

We performed an experimental dose study simulating a surgical procedure in children by performing thermoluminescent dosimeter (TLD) measurements in an anthropomorphic phantom (CIRS, Norfolk, Virginia), representing a genderless five-year-old child measuring 110 cm and weighing 19 kg.[24] The phantom is composed by tissue-equivalent epoxy resins, which offer tissue simulation. In addition, all bones are homogeneous and are formulated to represent age appropriate, average bone composition. The phantom is sectional in design with 25 mm thick sections, within holes providing TLDs locations specific to 22 inner organs. Its characteristics were in accordance with the specifications of the International Commission on Radiological Protection and the International Commission on Radiation Units and Measurements.[25,26]

To measure the absorbed doses (in Gy) in each organ, 31 TLDs (TLD Poland, Krakow, Poland) were placed inside the phantom turned to a prone position, as seen in Figure 1. Two additional TLDs were placed on the phantom's surface in order to measure the absorbed dose to the skin. The number of TLDs in each organ is summarized in Table 1. The unused holes were filled with adequate density plugs. The TLDs were prepared one day before measurements.

Irradiation settings

To perform the C-arm acquisitions we utilized the Ziehm Vision FD device (Ziehm Imaging, Nuremberg, Germany),[27] with the radiation beam centred to the pelvis. The focus to skin distance can vary, but is set to 75 cm in our case. The filtration is 3.9 mm aluminium plus 0.1 mm copper, and the detector size is 20 cm × 20 cm.

The O-arm surgical imaging system can generate 2D fluoroscopic and 3D volumetric images.[11] In 3D modality the tube-detector assembly rotates 360° around the patient and CT-like images of a 21 cm × 21 cm × 16 cm

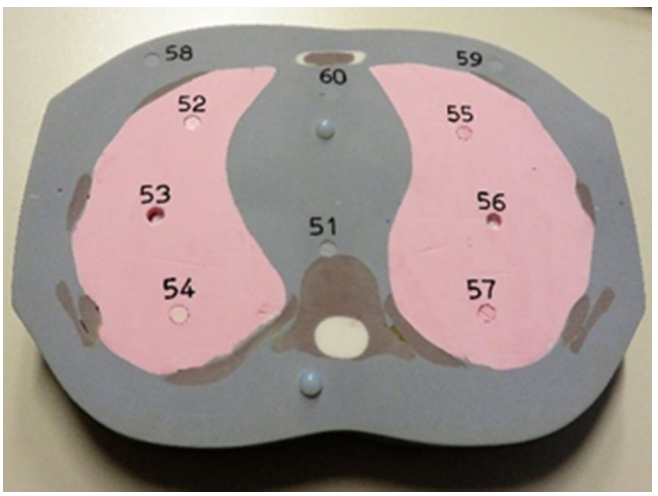

Fig. 1 Example of a phantom slice, showing different tissue densities, fixtures and thermoluminescent dosimeter placements with their associated number.

Table 1. The number of thermoluminescent dosimeters (TLDs) for each organ. Results of mean values of absorbed doses per one TLD with one 3D O-arm acquisition and one minute of C-arm for each organ of the phantom, and ratio between both methods (PA, posteroanterior).

Organ	Number of TLDs	One acquisition of O-arm in (µGy)	One minute of C-arm in (µGy)	O-arm /C-arm ratio	p (Student's t-test)
Far scattered radiation					**0.02**
Brain	2	0.86	0.15	5.73	
Left eye	1	1.03	0.04	26	
Right eye	1	1.16	0.27	4.3	
Thyroid	2	2.56	0.49	5.22	
Right lung	2	6.42	3.08	2.08	
Left lung	2	5.85	1.54	3.8	
Upper spine	1	4.29	1.66	2.58	
Close scattered radiation					**0.07**
Gallbladder	2	89.86	49.16	1.83	
Liver	5	36.41	21.32	1.7	
Intestine	3	114.85	55.34	2.08	
Pancreas	1	25.11	8.03	3.13	
Left kidney	1	26.3	8.32	3.16	
Direct radiation					**0.07**
Rectum	1	891.83	737.51	1.21	
Bladder	2	865.02	658.35	1.31	
Uterus/gonad	3	631.22	753.24	0.84	
Pelvic bone	2	559.57	463.79	1.21	
Skin entrance PA	2	1691.87	214.08	7.9	
Total	33		**Mean (sd)**	4.32 (5.89)	

volume are reconstructed (192 slices, 0.83 mm thickness, 512 × 512 matrix size) in 13 seconds. The O-arm has four patient sizes (S, M, L and XL) and four anatomical regions for its settings: extremities, chest, head and pelvis. These different regions are related to specific values of the tube voltage (kVp) and time–current product (mAs). The hip protocol was chosen for this study, with a small (S) patient size. The settings for voltage and time-current product were 80 kVp and 39 mAs, respectively. We utilized the O-arm with settings lower than the manufacturer's recommendations, in order to decrease the dose for the patient. At the end of a 3D acquisition, the O-arm displays the CT dose index ($CTDI_{vol}$) in mGy and the dose length product (DLP) in mGy.cm. The focus to skin distance is approximately 48 cm, the field size is fixed, the detector size is 40 cm × 30 cm and the filtration is unique and is set at 4 mm aluminium.

In order to obtain sufficient dose for each set of TLDs on the phantom, the first set was exposed to 30 3D acquisitions with the O-arm and the second set was exposed to ten minutes of 2D fluoroscopy with the C-arm (five minutes in posteroanterior (PA) and five minutes in lateral (LAT)). The cone-beam of the O-arm was centred on the pelvis. The absorbed doses of the TLDs were measured 48 hours after irradiation.

The results were normalized to one 3D acquisition of the O-arm and to one minute of fluoroscopy with the C-arm. When two or more TLDs were used for the same organ, we calculated the mean dose. Uncertainties were calculated at $k = 2$, according to the standard Guide to the Expression of Uncertainty in Measurement procedures.[28]

Table 2. Settings to evaluate different kerma rates at the skin entrance in the posteroanterior (PA) and lateral (LAT) orientations for the paediatric phantom on 2D mode.

Machine	Mode	Voltage (kV)		Current (mA)	
		PA	LAT	PA	LAT
O-arm	30 $p.s^{-1}$	65	71	9.2	9.6
C-arm	25 $p.s^{-1}$	64	72	3.4	5.7
C-arm	1 $p.s^{-1}$	63	72	3.4	5.9

For comparative purposes, we calculated the O-arm/C-arm dose ratio.

The O-arm surgical system can also perform 2D acquisitions. Dose rates were measured at the skin surface with both the O-arm in 2D fluoroscopy and the C-arm. These measurements were done using a 20X6-60E ionization chamber (Radcal, Monrovia, California),[29] placed on the source side perpendicular to incoming radiation. Ten seconds of fluoroscopy were done to allow the displayed rates on the probe to settle on both PA and LAT views. Dose output was expressed in $\mu G.s^{-1}$. The pulse frequency is fixed at 30 pulses/second ($p.s^{-1}$) for the O-arm. In automatic pulsed mode, the C-arm has a standard frequency of 25 $p.s^{-1}$ and automatically decreases to 8 $p.s^{-1}$ if no movement is detected. The 2D fluoroscopy of the O-arm was directly compared with different fluoroscopy modes available on a C-arm. These were investigated for both PA and LAT orientations. The parameters employed by the O-arm and the C-arm are summarized in Table 2.

To simulate the surgical procedure, all the devices were organized in an operating room, with typical set-up.

Statistical analysis

To compare irradiation level, we performed a Student's *t*-test with all the values of absorbed doses measured by the TLDs according to their position inside the phantom. The significance threshold was defined as 0.05.

Results

Patient exposure

Organ doses delivered for one 3D acquisition of the O-arm and those received after one minute of C-arm irradiation using PA and LAT orientations are shown in Figure 2 and Table 1. Three main regions were observed according to the distance from the isocentre of the irradiation: direct (coloured in red in Figure 2) such as pelvic organs, close scattered (coloured in yellow) such as abdominal and retroperitoneal organs, and far scattered radiations (coloured in blue) such as thoracic, head and neck organs.

All radiation doses were expressed in µGy. We found that doses varied from 631.22 to 1691.87 with the O-arm and from 214.08 to 737.51 for the C-arm, without significant difference (p = 0.07). Close scattered radiation doses were ranged from 25.11 to 114.85 for the O-arm

JOURNAL OF CHILDREN'S ORTHOPAEDICS

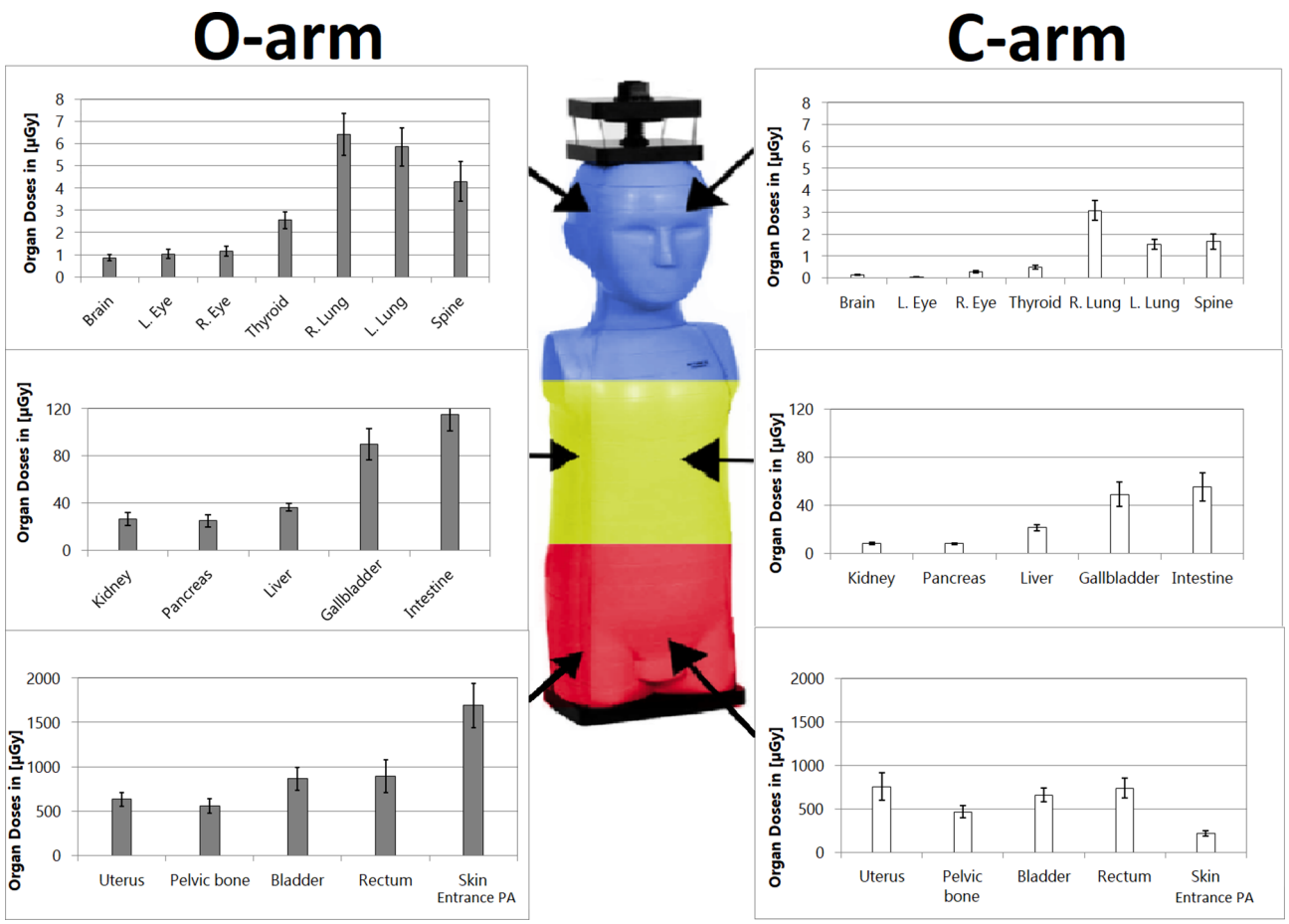

Fig. 2 Absorbed doses comparison for each organ between one 3D acquisition with the O-arm and one minute of fluoroscopy with the C-arm. Direct irradiation on the pelvic organs is coloured by red. Scattered irradiation on abdominal organs is coloured yellow and on thoracic and upper organs blue, with decreasing level respectively (R., right; L., left; PA, posteroanterior).

and from 8.03 to 55.34 for the C-arm, without any significant difference ($p = 0.07$). Far scattered radiation doses varied from 0.86 to 6.42 for the O-arm and from 0.04 to 3.08 for the C-arm, and showed a significant difference ($p = 0.02$).

The lowest dose for one 3D acquisition with the O-arm was 0.86 for the brain. In comparison, the same organ received a mean 0.15 with one minute of C-arm fluoroscopy. The O-arm/C-arm ratio was 5.73.

The highest dose with the O-arm was for the skin, with a mean value of 1691.87. With the C-arm, this absorbed dose was a mean 214.08. So, the O-arm/C-arm ratio was 7.90.

Incident dose at the skin surface on 2D mode

The C-arm consistently provided a lower dose output due to its lower pulse frequency used compared with the O-arm and to the larger focus–skin distance. The value observed for the O-arm in PA was 328.83 µGy.s^{-1}, but only 1.90 µGy.s^{-1} with the C-arm (Fig. 3).

Discussion

The most important finding of the present study is that the mean irradiation level is approximately four times higher for one 3D acquisition of the O-arm than for one minute of C-arm. As expected, the mean absorbed doses were higher in the field of imaging (centred by the pelvis) because of direct incidence of the radiation beam. In this region, coloured in red in Figure 2, the absorbed doses were similar with a mean O-arm/C-arm ratio around 1, except for the skin entrance with a ratio of almost 8. The further the organs were from the isocentre of the beam, the more this ratio increased, with a mean of about 3 for abdominal and retroperitoneal organs (coloured in yellow in Figure 2), and from 5 to 26 for the left eye (coloured in blue in Figure 2) with significant difference in doses for far scattered irradiation. So, scattered irradiation level was clearly higher with the O-arm, but direct irradiation level was similar with both imaging techniques.

The left–right asymmetry observed in cases of the C-arm, right doses larger than left doses for the organs,

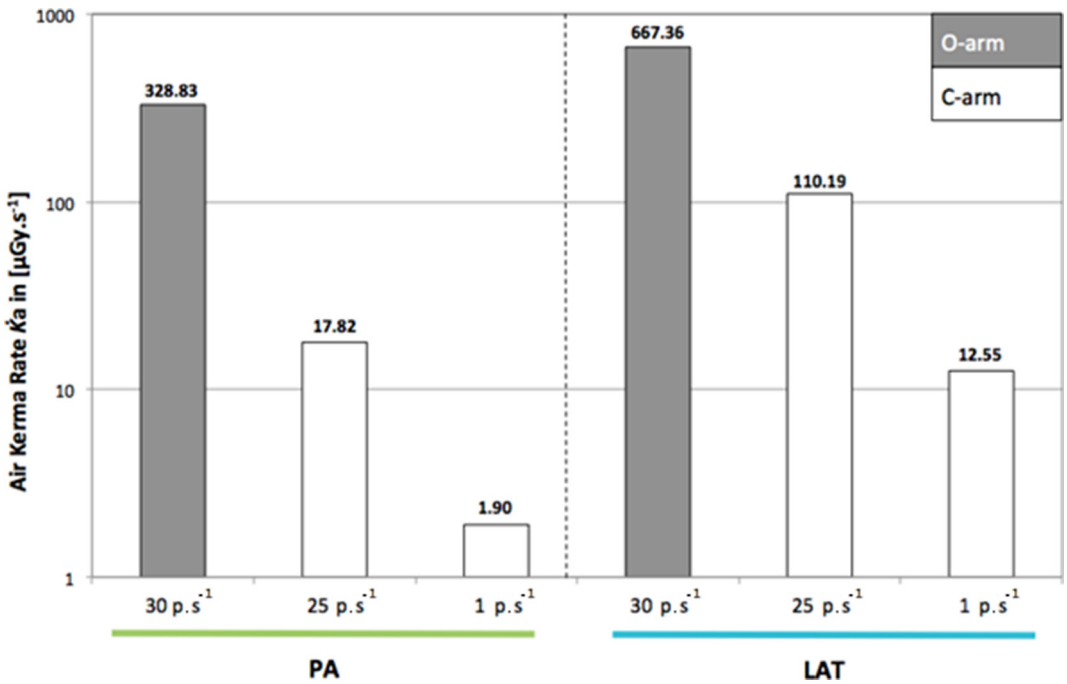

Fig. 3 Comparison of dose output (air kerma rate) at the skin surface with the O-arm in 2D mode and with the C-arm for both ten seconds of fluoroscopy (PA, posteroanterior; LAT, lateral).

came from the fact that the radiation field when using two specific projections was not homogenous, and the LAT employed in this study delivered higher radiation to the organs placed at the right side of the patient (right lung, right eye), due to the position of the X-ray tube. This inhomogeneity was also the cause for observing higher dose at the uterus level. Indeed for the uterus three TLDs were placed, one at the centre and two off-centre. The one placed at the right side of the patient by its very short distance to the tube when working in LAT position has received a very high dose, increasing the overall mean dose value for this organ.

To our knowledge, dosimetric studies of the O-arm surgical system are rarely published, especially in paediatrics. However for adults, Pitteloud et al[19] characterized the dosimetric properties of the O-arm in the same conditions as our study. Doses delivered by the O-arm to the paediatric phantom were lower than those delivered to the adult phantom. For example, the mean dose to the brain was 4 µGy for the adult, but only 0.86 µGy in our paediatric case, with the beam centred on the pelvis. This was attributed to the lower tube voltage and current, resulting in a less energetic and intense field. This was expected as the radiation passes through less material when compared with the adult phantom.

Furthermore, the O-arm gives the $CTDI_{vol}$ and the DLP ($CTDI_{vol}$ × scan length) at the end of each acquisition. For reference, according to Zhang et al,[30] the patient dose delivered by the O-arm in default mode is equivalent to 0.5 to 0.6 times the dose delivered by a conventional 64 slice CT-scanner. Comparing with our results, the $CTDI_{vol}$ for the O-arm was more than eight times higher in adults in the study from Pitteloud et al[19] in comparison with our paediatric phantom (Table 3).

Table 3. Comparison of mean $CTDI_{vol}$ level of one O-arm acquisition between adult from Pitteloud et al[19] and paediatrics with our results

Adult $CTDI_{vol}$ (mGy)	Paediatric $CTDI_{vol}$ (mGy)	Adult/paediatric ratio
8.83	1.02	8.66

Su et al[20] evaluated the accuracy in pedicle screw placement for adolescent idiopathic scoliosis and the resulting effective doses. They reported a mean total effective dose for the O-arm group significantly and approximately four times higher than that of the C-arm group, which was similar to our mean result of 4.32. Other authors studied the effective dose in children with pedicle screw placement.[18] They found a mean O-arm/C-arm ratio of 4.24, which was also similar to ours.

Computed surgery navigation to guide the surgeon has existed for more than ten years. It is usually utilized in adult orthopaedic surgery, especially in primary total knee arthroplasty, in order to guide the cut heights and rotations to restore the normal mechanical axis.[31] They provide a help during the surgery without additional imaging acquisition. In children, the surgical navigation can be used in spine surgery, like for O'Donnell et al[32] who compared the average effective dose by C-arm and free-hand technique *versus* computerized navigation in posterior fusion. They reported a mean effective dose of 0.189 mSv with the C-arm and 7.29 mSv per case with the

O-arm-navigation, which generated an O-arm/C-arm ratio of 38.6, a result higher than ours and other publications.

Several authors reported good results with the navigation system on osteoid osteoma resection[33-38] and growth modulation.[39] Others studied the slipped femoral capitis epiphysis and found promising results provided by the navigation system in cervical femoral screw placement with higher accuracy using the navigation.[40]

Some of these surgical procedures could benefit from the help of surgical navigation in order to perform more minimally-invasive and more accurate procedures. The radiation exposure with the O-arm was consistently higher than with the C-arm, even with paediatric low-dose settings, especially regarding scattered radiation. The 3D imaging is necessary for navigation use. New generations of 3D C-arms are making their way into our operating rooms. However, the O-arm remains the most current 3D imaging system available.

According to our results, the absorbed skin doses were systematically higher with the O-arm in 2D mode, from six to 164 times the doses of the C-arm. These results were previously highlighted by a study from Nelson et al[41] which reported doses 38 times higher with the O-arm for LAT view and 54 times higher for anteroposterior view than with the C-arm. This indicates the need to avoid the 2D mode of the O-arm, even with the difficulty of having two devices if a 2D control after 3D O-arm utilization during the same surgical procedure is required.

The observed dose difference is attributed to a lower tube current, which is automatically regulated by the machines for a given voltage and also due to the frequency rate of the pulses. The frequency is fixed at 30 $p.s^{-1}$ in the O-arm. For orthopaedic surgery there is no need to use a frequency of 25 $p.s^{-1}$ (automatic mode) or higher, because no continuous movement has to be visualized. Pulse frequency can be reduced to 1 $p.s^{-1}$, giving the advantage of decreasing the exposure of the skin.

Moreover, when comparing the dose rate at the surface of the skin with the adult phantom,[19] the difference was lower on the paediatric phantom by a factor almost ten. The C-arm consistently had a lower dose rate. The largest difference was observed in PA where the dose rate for the O-arm was 328.83 $\mu Gy.s^{-1}$, but only 1.90 $\mu Gy.s^{-1}$ with the C-arm. This implies that using the C-arm in PA for almost three minutes will expose the skin of the patient at the same dose as one second of O-arm in 2D mode.

The major limit of our study was the duration of one minute of C-arm for comparison with one acquisition with the O-arm. This decision was determined on one hand by empiric experience of C-arm intraoperative utilization, and on the other hand by the literature.[20] Additionally, we performed a lab study on a phantom, and not on living patients. We also measured the absorbed dose to the organs, not the effective dose, which is more predictable for radiation-induced cancer risk.[1] However, as the effective dose is a weighted summation of absorbed dose to different organs, lower doses to the organs correlates with a lower effective dose. Dosimetry quantifies patient exposure through measurements of estimated radiation-induced injuries such as deterministic effects (with a threshold limit of 0.5 Gy, especially for the skin where erythema can appear from 2 Gy) and stochastic effects (probability for radiation-induced cancer, which is overall 5% per Sv per year for an adult and between two to four times higher for a child).[1,42] Considering our maximum dose value to the skin of 1691.87 µGy = 1,7 10^{-6} Gy, the results were far away from deterministic effects in our study.

Thus, according to the Beir VII publication, the linear no-threshold model was utilized to predict radiation-induced cancer risk and considered to be the most acceptable description.[1] We highlight the need to know the dosimetry of an imaging system, because of its importance for optimizing patient safety.[43]

Conclusion

Absorbed doses to the organs for one minute of fluoroscopy with the C-arm were found to be lower than those for a single 3D O-arm acquisition, with a mean O-arm/C-arm ratio of 4.32. During a pelvic irradiation, absorbed doses to the organs for a 3D O-arm acquisition were higher than with one minute of fluoroscopy with the C-arm, but with a significant difference observed only for thoracic, neck and head organs (far scattered radiation).

Dose rates at the surface of the skin were also consistently lower with the C-arm than with the O-arm.

Imaging durations from which typical durations can be extracted should be kept in records, for example in the Digital Imaging and Communications in Medicine (DICOM) header or in the Picture Archiving and Communication System (PACS) systems. We plan to perform a clinical study assessing current radiation exposure, collecting data especially important in paediatric orthopaedics.

Received 07 February 2018; accepted after revision 19 July 2018.

COMPLIANCE WITH ETHICAL STANDARDS

FUNDING STATEMENT

No benefits in any form have been received or will be received from a commercial party related directly or indirectly to the subject of this article.

OA LICENCE TEXT

This article is distributed under the terms of the Creative Commons Attribution-Non Commercial 4.0 International (CC BY-NC 4.0) licence (https://creativecommons.org/licenses/by-nc/4.0/) which permits non-commercial use, reproduction and distribution of the work without further permission provided the original work is attributed.

ETHICAL STATEMENT

Ethical approval: This article does not contain any studies with human participants or animals performed by any of the authors.
Informed consent: Not required.

REFERENCES

1. **National Research Council**. Health risks from exposure to low levels of ionizing radiation: BEIR VII phase 2. *National Academies Press* 2006 April 23.

2. **Kleinerman RA.** Cancer risks following diagnostic and therapeutic radiation exposure in children. *Pediatr Radiol* 2006;36:121-125.

3. **Shore RE, Hildreth N, Dvoretsky P, et al.** Thyroid cancer among persons given X-ray treatment in infancy for an enlarged thymus gland. *Am J Epidemiol* 1993;137:1068-1080.

4. **Preston DL, Mattsson A, Holmberg E, et al.** Radiation effects on breast cancer risk: a pooled analysis of eight cohorts. *Radiat Res* 2002;158:220-235.

5. **Karlsson P, Holmberg E, Lundell M, et al.** Intracranial tumors after exposure to ionizing radiation during infancy: a pooled analysis of two Swedish cohorts of 28,008 infants with skin hemangioma. *Radiat Res* 1998;150:357-364.

6. **Shore RE, Moseson M, Xue X, et al.** Skin cancer after X-ray treatment for scalp ringworm. *Radiat Res* 2002;157:410-418.

7. **Infante-Rivard C, Mathonnet G, Sinnett D.** Risk of childhood leukemia associated with diagnostic irradiation and polymorphisms in DNA repair genes. *Environ Health Perspect* 2000;108:495-498.

8. **Smith-Bindman R, Lipson J, Marcus R, et al.** Radiation dose associated with common computed tomography examinations and the associated lifetime attributable risk of cancer. *Arch Intern Med* 2009;169:2078-2086.

9. **Ron E.** Cancer risks from medical radiation. *Health Phys* 2003;85:47-59.

10. **Zhu W, Sun W, Xu L, et al.** Minimally invasive scoliosis surgery assisted by O-arm navigation for Lenke Type 5C adolescent idiopathic scoliosis: a comparison with standard open approach spinal instrumentation. *J Neurosurg Pediatr* 2017;19:472-478.

11. **Medtronic.** O-arm user manual, MN. http://www.medtronic.com/content/dam/medtronic-com/us-en/newsroom/media-resources/media-kits/o-arm-imaging-system/documents/O-Arm%20Backgrounder.pdf (date last accessed 11 December 2017).

12. **Medtronic.** StealthStation user manual, MN. http://www.medtronic.com/us-en/healthcare-professionals/products/spinal-orthopaedic/surgical-navigation-imaging/spine-surgery-imaging-surgical-navigation/manuals-technical-resources.html (date last accessed 11 December 2017).

13. **Jin M, Liu Z, Liu X, et al.** Does intraoperative navigation improve the accuracy of pedicle screw placement in the apical region of dystrophic scoliosis secondary to neurofibromatosis type I: comparison between O-arm navigation and free-hand technique. *Eur Spine J* 2016;25:1729-1737.

14. **Van de Kelft E, Costa F, Van der Planken D, Schils F.** A prospective multicenter registry on the accuracy of pedicle screw placement in the thoracic, lumbar, and sacral levels with the use of the O-arm imaging system and StealthStation Navigation. *Spine* 2012;37:E1580-E1587.

15. **Su AW, Luo TD, McIntosh AL, et al.** Switching to a pediatric dose O-arm protocol in spine surgery significantly reduced patient radiation exposure. *J Pediatr Orthop* 2016;36:621-626.

16. **Abul-Kasim K, Söderberg M, Selariu E, et al.** Optimization of radiation exposure and image quality of the cone-beam O-arm intraoperative imaging system in spinal surgery. *J Spinal Disord Tech* 2012;25:52-58.

17. **Petersen AG, Eiskjær S, Kaspersen J.** Dose optimisation for intraoperative cone-beam flat-detector CT in paediatric spinal surgery. *Pediatr Radiol* 2012;42:965-973.

18. **Dabaghi Richerand A, Christodoulou E, Li Y, et al.** Comparison of effective dose of radiation during pedicle screw placement using intraoperative computed tomography navigation versus fluoroscopy in children with spinal deformities. *J Pediatr Orthop* 2016;36:530-533.

19. **Pitteloud N, Gamulin A, Barea C, et al.** Radiation exposure using the O-arm® surgical imaging system. *Eur Spine J* 2017;26:651-657.

20. **Su AW, McIntosh AL, Schueler BA, et al.** How does patient radiation exposure compare with low-dose o-arm versus fluoroscopy for pedicle screw placement in idiopathic scoliosis? *J Pediatr Orthop* 2017;37:171-177.

21. **Rampersaud YR, Foley KT, Shen AC, Williams S, Solomito M.** Radiation exposure to the spine surgeon during fluoroscopically assisted pedicle screw insertion. *Spine* 2000;25:2637-2645.

22. **Rehani MM, Ciraj-Bjelac O, Vañó E, et al.** ICRP Publication 117. Radiological protection in fluoroscopically guided procedures performed outside the imaging department. *Ann ICRP* 2010;40:1-102.

23. **National Council on Radiation Protection and Measurements**. Radiation dose management for fluoroscopically guided interventional medical procedures. Bethesda, MD: *NCRP* 168;2010.

24. **CIRS**. ATOM dosimetry phantoms, VA. http://www.cirsinc.com/file/Products/701_706/701%20706%20ATOM%20PB%20110615.pdf (date last accessed 11 December 2017).

25. **International Commission on Radiological Protection**. Report on the task group on reference man. Publication 23, Ottawa. http://journals.sagepub.com/doi/pdf/10.1016/S0074-2740%2875%2980015-8 (date last accessed 11 December 2017).

26. **ICRU.** P. computational models in Therapy, Diagnosis and Protection. *International Commission on Radiation Units and Measurements Report*. 1992;48.

27. **Ziehm Imaging**. Ziehm Vision 26366-5_4.12_EN_00, user manual. http://www.wemed1.com/downloads/dl/file/id/7960/product/10537/manual_for_xrc_z_vision_r.pdf (date last accessed 11 December 2017).

28. **Joint Committee for Guides in Metrology.** Guide to the expression of uncertainty in measurement. International Organization for Standardization, Geneva. https://www.bipm.org/utils/common/documents/jcgm/JCGM_100_2008_E.pdf (date last accessed 11 December 2017).

29. **RadCal**. 20X6 Chambers - Technical Specifications. http://www.testmart.com/webdata/mfr_pdfs/RADCAL/ew-20x6-chamber-spec-sheet-web-11-2-28.pdf (date last accessed 11 December 2017).

30. **Zhang J, Weir V, Fajardo L, et al.** Dosimetric characterization of a cone-beam O-arm imaging system. *J Xray Sci Technol* 2009;17:305-317.

31. **Cheng T, Zhao S, Peng X, Zhang X.** Does computer-assisted surgery improve postoperative leg alignment and implant positioning following total knee arthroplasty? A meta-analysis of randomized controlled trials? *Knee Surg Sports Traumatol Arthrosc* 2012;20:1307-1322.

32. **O'Donnell C, Maertens A, Bompadre V, Wagner TA, Krengel W III.** Comparative radiation exposure using standard fluoroscopy versus cone-beam computed tomography for posterior instrumented fusion in adolescent idiopathic scoliosis. *Spine* 2014;39:E850-E855.

33. **Widmann G, Schullian P, Fasser M, Niederwanger C, Bale R.** CT-guided stereotactic targeting accuracy of osteoid osteoma. *Int J Med Robot* 2013;9:274-279.

34. **Reverte-Vinaixa MM, Velez R, Alvarez S, Rivas A, Perez M.** Percutaneous computed tomography-guided resection of non-spinal osteoid osteomas in 54 patients and review of the literature. *Arch Orthop Trauma Surg* 2013;133:449-455.

35. **Rajasekaran S, Karthik K, Chandra VR, Rajkumar N, Dheenadhayalan J.** Role of intraoperative 3D C-arm-based navigation in percutaneous excision of osteoid osteoma of long bones in children. *J Pediatr Orthop B* 2010;19:195-200.

36. **Rajasekaran S, Kamath V, Shetty AP.** Intraoperative Iso-C three-dimensional navigation in excision of spinal osteoid osteomas. *Spine* 2008;33:E25-E29.

37. **Neumann D, Berka H, Dorn U, Neureiter D, Thaler C.** Follow-up of thirty-three computed-tomography-guided percutaneous radiofrequency thermoablations of osteoid osteoma. *Int Orthop* 2012;36:811-815.

38. **Outani H, Hamada K, Takenaka S, et al.** Radiofrequency ablation of osteoid osteoma using a three-dimensional navigation system. *J Orthop Sci* 2016;21:678-682.

39. **Dong Y, Lü X, Zhang J, Guo Y.** Clinical application of computer navigation in physeal bridge resection in pediatric partial epiphyseal plate closure. *Zhonghua Yi Xue Za Zhi* 2014;94:1631-1634.

40. **Bono KT, Rubin MD, Jones KC, et al.** A prospective comparison of computer-navigated and fluoroscopic-guided in situ fixation of slipped capital femoral epiphysis. *J Pediatr Orthop* 2013;33:128-134.

41. **Nelson EM, Monazzam SM, Kim KD, Seibert JA, Klineberg EO.** Intraoperative fluoroscopy, portable X-ray, and CT: patient and operating room personnel radiation exposure in spinal surgery. *Spine J* 2014;14:2985-2991.

42. **ORaP RO814**. Ordonnance sur la radioprotection. https://www.admin.ch/opc/fr/classified-compilation/19940157/index.html (date last accessed 11 December 2017).

43. **Hadelsberg UP, Harel R.** Hazards of ionizing radiation and its impact on spine surgery. *World Neurosurg* 2016;92:353-359.